Dual Two-Level Converters Based on Direct Power Control for an Open-Winding Brushless Doubly-Fed Reluctance Generator

Shi Jin, *Member, IEEE*, Long Shi, Liancheng Zhu, Wenping Cao, *Senior Member, IEEE*, Ting Dong, and Fengge Zhang, *Member, IEEE*

***Abstract*—This paper proposes a novel open-winding brushless doubly-fed reluctance generator (OW-BDFRG) with dual two-level converters in order to reduce the converter rating and switching frequency for large-scale wind turbine applications. The new converter topology is equivalent to a three-level converter directly connected to the control winding of typical BDFRG. The OW-BDFRG system with this topology structure requires lower converter rating and switching frequency, and has a more flexible control mode, better operation performance, and fault redundancy capability. For the OW-BDFRG, this paper also proposes a new control scheme combining direct power control (DPC) with sliding mode variable structure (SMVS) control to implement the power tracking. The voltage-vector switching table of DPC is redesigned according to the error signals of active and reactive powers of the power winding, as well as the sector location of control winding flux. The active and reactive powers of the OW-BDFRG can be directly decoupled and independently controlled by properly selecting the switching voltage vectors. The novelty of this paper lies in an OW-BDFRG topology driven by dual two-level converters to improve the system characteristics, and the use of SMVS control to improve the DPC accuracy and robustness to parameter variations. Finally, the effectiveness of the proposed system is verified through simulation and experimental studies.**

***Index Terms*—Brushless doubly-fed generator (BDFG), direct power control (DPC), dual two-level converter, open-winding structure, reluctance rotor, sliding mode variable structure (SMVS).**

Manuscript received October 17, 2016; revised February 21, 2017; accepted April 2, 2017. Date of publication April 12, 2017; date of current version July 15, 2017. Paper 2016-SECSC-1075.R1, presented at the 2016 IEEE Transportation Electrification Conference and Exposition, Asia-Pacific, Busan, South Korea, Jun. 1–4, 2016, and approved for publication in the IEEE TRANSACTIONS ON INDUSTRY APPLICATIONS by the Sustainable Energy Conversion Systems Committee of the IEEE Industry Applications Society. This work was supported in part by the National Natural Science Foundation of China under Grant 51537007 and Grant 51277124, and in part by the Natural Science Foundation of Liaoning Province, China, under Grant 201602540. *(Corresponding author: Shi Jin.)*

S. Jin, L. Shi, T. Dong, and F. Zhang are with Shenyang University of Technology, Shenyang 110870, China (e-mail: wby-js@163.com; 1914767155@qq.com; tina_dong1111@163.com; zhangfg@sut.edu.cn).

L. Zhu is with the Shenyang University of Technology, Shenyang 110870, China, and also with the University of Science and Technology Liaoning, Anshan 114051, China (e-mail: zhuliancheng@163.com).

W. Cao is with Aston University, Birmingham B4 7ET, U.K. (e-mail: w.p.cao@aston.ac.uk).

Color versions of one or more of the figures in this paper are available online at http://ieeexplore.ieee.org.

Digital Object Identifier 10.1109/TIA.2017.2693959

I. INTRODUCTION

THE BRUSHLESS doubly-fed reluctance generator (BDFRG) has advantages of high reliability with a brushless structure, low converter rating and cost, and adjustable active and reactive powers, making it particularly suited for variable-speed large-scale wind power applications [1]–[3]. The typical BDFRG has two sets of three-phase windings on the stator (a control winding for excitation and a power winding for power generation) with two different pole numbers. The two windings are magnetically coupled through a special reluctance rotor [4].

The converter for the BDFRG deals with the slip power in the machine, so that the converter rating can be reduced, so is the converter cost. For further reducing the converter capacity and system cost to adapt to the requirement of the large wind turbines, an open-winding brushless doubly-fed reluctance generator (OW-BDFRG) is proposed in this paper. Its control winding uses an open-winding structure and all the six terminals are pulled out for control purposes. The two ends of the control winding are connected across dual two-level converters with the isolated dc bus connection mode to supply. This topology is equivalent to a three-level converter directly connected to the control winding of the typical BDFRG, and can solve the unbalanced-voltage-division problem of dc capacitor in the three-level converter. Since the full dc bus voltage can be directly applied to a single phase rather than across two phases, the dc bus voltage as well as the device voltage rating can be significantly lowered [5]. Each phase current in the three-phase control winding can be independently controlled. So this topology structure enables the brushless doubly-fed wind power generation system to have smaller converter capacity, lower switching frequency, more flexible control mode, and better operation performance and fault redundancy capability. The open-winding structure has been applied to the permanent magnet synchronous generator to adapt to the trend of the larger and larger unit capacity in the modern wind power generation system [6]–[9].

Another issue of the BDFRG is the power tracking control to improve the generation efficiency. In the literature, field-oriented control is mainly adopted to decouple and independently control the active and reactive powers for this purpose [10]–[15]. But it requires a complex coordinate transformation and a massive calculation resource. Moreover, it is vulnerable to generator parameter variations so that the system robustness is low. Some scholars have attempted to apply direct torque control (DTC) for variable-speed constant-frequency BDFRG [16]–[20]. Compared with the field-oriented control, DTC without field orientation and coordinate transformation has a simpler structure, faster dynamic response, and better robustness. However, its flux observer is sensitive to generator parameter variations and inaccurate identification, especially in the case of low excitation current frequency of control winding, which results in the worse real-time of control system. Alternatively, direct power control (DPC), derived from DTC [21], can directly decouple and independently control active and reactive powers. Compared with DTC, DPC has a simpler algorithm, less calculation, and does not need to measure the flux amplitude, which can well solve the problem of the worse real-time of control system caused by the flux observer being sensitive to generator parameter variations. Therefore, DPC is found in use in brushless doubly-fed motor systems [22].

In this paper, the dual two-level converters are employed to drive the proposed OW-BDFRG whereas a combination of DPC control and sliding mode variable structure (SMVS) [23]–[24] is developed to implement the power tracking and improve the control accuracy and robustness. Finally, the whole system is tested by simulation and experimental methods.

II. Structure and Model of the OW-BDFRG

A. System Structure

A schematic diagram of the proposed OW-BDFRG wind power system is shown in Fig. 1. In the stator, the power winding is directly connected to the grid. The control winding has an open-winding structure, that is, the control winding is completely opened and the six terminals are all drawn out. The two ends of the control winding are connected to the dual two-level bidirectional converters.

B. Generator Model

The voltages and fluxes of the OW-BDFRG in the two-phase stationary reference frame are expressed as

$$\begin{bmatrix} u_{p\alpha} \\ u_{p\beta} \\ u_{c\alpha} \\ u_{c\beta} \end{bmatrix} = \begin{bmatrix} R_p + L_p D & -\omega_p L_p & L_m D & \omega_p L_m \\ \omega_p L_p & R_p + L_p D & \omega_p L_m & -L_m D \\ L_m D & \omega_c L_m & R_c + L_c D & -\omega_c L_c \\ \omega_c L_m & -L_m D & \omega_c L_c & R_c + L_c D \end{bmatrix} \cdot \begin{bmatrix} i_{p\alpha} \\ i_{p\beta} \\ i_{c\alpha} \\ i_{c\beta} \end{bmatrix} \quad (1)$$

$$\begin{bmatrix} \Psi_{p\alpha} \\ \Psi_{p\beta} \\ \Psi_{c\alpha} \\ \Psi_{c\beta} \end{bmatrix} = \begin{bmatrix} L_p & 0 & L_m & 0 \\ 0 & L_p & 0 & -L_m \\ L_m & 0 & L_c & 0 \\ 0 & -L_m & 0 & L_c \end{bmatrix} \cdot \begin{bmatrix} i_{p\alpha} \\ i_{p\beta} \\ i_{c\alpha} \\ i_{c\beta} \end{bmatrix} \quad (2)$$

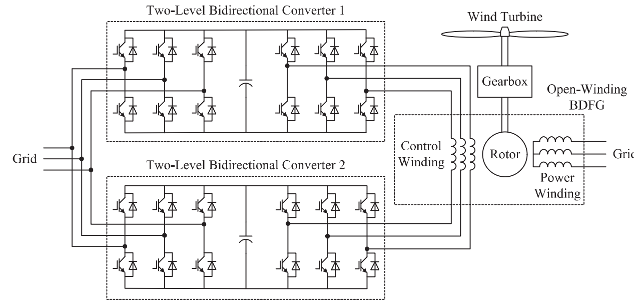

Fig. 1. Schematic diagram of the proposed OW-BDFRG.

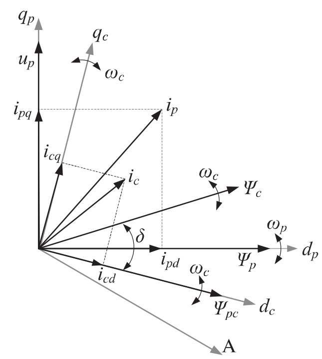

Fig. 2. Phasor diagram of the OW-BDFRG.

where *u* is the voltage, *i* is the current, Ψ is the flux, *R* is the resistance, L_p, L_c, and L_m are the self-inductance of the power winding, self-inductance of the control winding, and the mutual inductance between the power winding and control winding, respectively, and ω is the electrical angular. The subscript *p* represents the power winding, *c* represents the control winding, *r* represents the rotor winding, α represents the α-axis component, β represents the β-axis component, and *D* represents the differential operator.

For OW-BDFRG system with the dual two-level converters and isolated dc bus connection mode structure, the control winding voltages $u_{c\alpha}$ and $u_{c\beta}$ are the differences between the output voltages of the dual two-level converters, respectively,

$$\begin{cases} u_{c\alpha} = u_{c\alpha 1} - u_{c\alpha 2} \\ u_{c\beta} = u_{c\beta 1} - u_{c\beta 2} \end{cases}. \quad (3)$$

The active power P_{p} and reactive power Q_{p} can be expressed as

$$\begin{cases} P_p = \dfrac{3}{2}\left(u_{p\alpha} i_{p\alpha} + u_{p\beta} i_{p\beta}\right) \\ Q_p = \dfrac{3}{2}\left(u_{p\beta} i_{p\alpha} - u_{p\alpha} i_{p\beta}\right) \end{cases}. \quad (4)$$

According to the OW-BDFRG model, the power winding flux Ψ_p is chosen to coincide with the *d*-axis in the power winding *d*-*q* reference frame. $\Psi_p = \Psi_{pd}$ and $\Psi_{pq} = 0$, Also neglecting the stator winding resistance, the phasor diagram of the OW-BDFRG is obtained as Fig. 2, where Ψ_{pc} is the flux of the

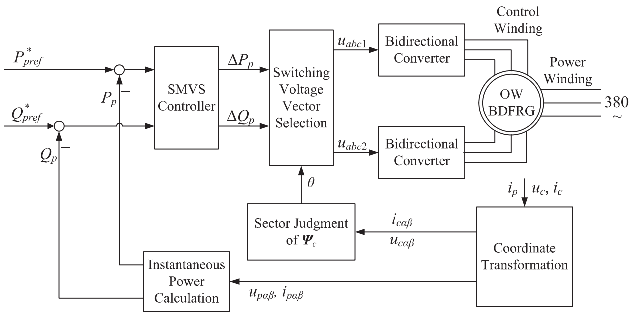

Fig. 3. Diagram of SMVS-enhanced DPC.

power winding linking the control winding, and its amplitude $\Psi_{pc} = \frac{L_m}{L_p}\Psi_p$.

III. SMVS-Enhanced DPC Control

A. Control Principles

DPC is derived from DTC idea. The principle diagram of SMVS-enhanced DPC is obtained referring to DTC, shown in Fig. 3, where P^*_{pref} and Q^*_{pref} are the reference active and reactive powers, respectively, and ΔP_p and ΔQ_p are the errors in active and reactive powers, respectively. The voltage-vector switching table of DPC is redesigned based on the error signals of active and reactive powers of power winding as well as the sector location of the control winding flux. The active and reactive powers of OW-BDFRG can be directly decoupled and independently controlled by properly selecting the switching voltage vectors. The SMVS control is introduced into DPC to minimize the tracking errors in the active and reactive powers.

The electromagnetic torque T_{e} of the OW-BDFRG is induced by the interaction between the fluxes Ψ_{pc} and Ψ_c from Fig. 2, i.e.,

$$T_e = \frac{3(p_p + p_c)L_p}{2(L_p L_c - L_m^2)} |\boldsymbol{\Psi}_c| |\boldsymbol{\Psi}_{pc}| \sin\delta. \tag{5}$$

For the large-scale OW-BDFRG, its stator winding resistance can usually be neglected. In the absence of copper loss, the electromagnetic power is approximately equal to the output power, that is, $P_{pe} \approx P_{po}$. The amplitude of the power winding flux Ψ_p is approximately constant because the power winding is connected to the grid, so Ψ_{pc} is also approximately constant. The electromagnetic torque T_{e} can be adjusted by changing the flux angle δ, so long as the amplitude of the control winding flux Ψ_c is kept to be constant. The active power P_p is a function of the electromagnetic torque T_{e}, so the active power P_p can be controlled by changing the flux angle δ, referring to as the torque control method. Since both stator windings contribute to the establishment of the airgap flux, it is natural that if one winding contributes more, the other should contribute less. Therefore, the reactive power Q_p can be controlled by the flux amplitude of the control winding Ψ_c. According to the above analysis, the voltage-vector switching table of DPC can be redesigned based on the changes of P_p and Q_p.

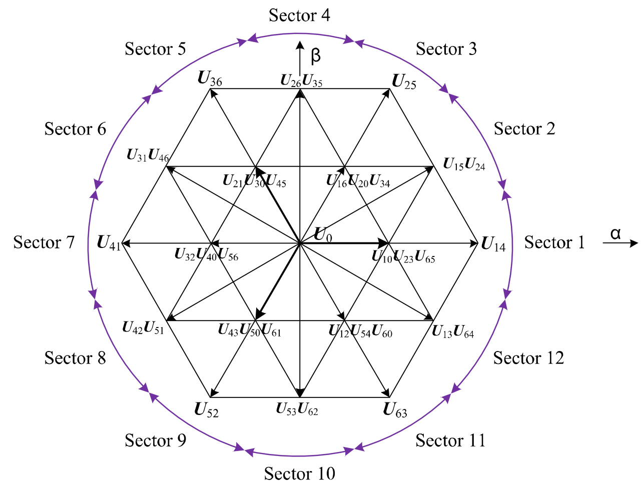

Fig. 4. Voltage-vector switching diagram and sector division.

B. Sector Division and Voltage-Vector Switching Selection

Since the control winding of the OW-BDFRG is fed from dual two-level converters, more than doubled switching voltage vectors are produced than a typical converter. In this case, subdividing the vector sectors is necessary to select more switching voltage vectors for more accurate control. The whole vector plane is equally divided into 12 sectors. According to (3), the switching voltage vectors and sector division are obtained by the parallelogram rule of voltage vector composition, as shown in Fig. 4, where U_{mn} represents the composition of the voltage vector U_m produced by converter 1 and U_n produced by converter 2.

From Fig. 4, these voltage vectors can be divided into six long vectors, six medium vectors, six short vectors, and zero vectors, according to their relative amplitudes. If the control winding of OW-BDFRG is fed with different voltage vectors, the change of active and reactive powers can be different referring to as the analysis in Section III-A. In practice, there are three main methods of selecting voltage vectors: long vector, medium vector, and hybrid vector. The long vectors of DPC method are obtained when both the two-level converters output the vectors with an opposite direction according to (3), including the vectors $\boldsymbol{U}_{14}, \boldsymbol{U}_{25}, \boldsymbol{U}_{36}, \boldsymbol{U}_{41}, \boldsymbol{U}_{52}$ and $\boldsymbol{U}_{63}$ in Fig. 4. The medium vectors of DPC method are gotten when both the two-level converters output the vectors with an angle of 120° (between two adjacent long vectors), including the vectors $\boldsymbol{U}_{15}/\boldsymbol{U}_{24}$, $\boldsymbol{U}_{26}/\boldsymbol{U}_{35}$, $\boldsymbol{U}_{31}/\boldsymbol{U}_{46}$, $\boldsymbol{U}_{42}/\boldsymbol{U}_{51}$, $\boldsymbol{U}_{53}/\boldsymbol{U}_{62}$ and $\boldsymbol{U}_{13}/\boldsymbol{U}_{64}$ in Fig. 4. Thus, these two methods can only utilize six voltage vectors and lack the control flexibility. In addition, they suffer from power overshooting. Alternatively, a hybrid-vector DPC method combines both long vectors and medium vectors produced by the dual two-level converters. This method can yield more switching voltage vectors and has better controllability and lower switching frequency than the first two methods. It is thus adopted in this paper for selecting switching voltage vectors. For example, if the control winding flux $\boldsymbol{\Psi}_c$ locates at Section I in Fig. 4, $\Delta P_p > 0$ and $\Delta Q_p > 0$,

TABLE I
VOLTAGE-VECTOR SELECTION TABLE FOR THE HYBRID-VECTOR DPC

Error		Sector											
$\Delta P_p = P^*_{p\mathrm{ref}} - P_p$	$\Delta Q_p = Q^*_{p\mathrm{ref}} - Q_p$	1	2	3	4	5	6	7	8	9	10	11	12
$\Delta P_p > 0$	$\Delta Q_p > 0$	$\boldsymbol{U}_{31}$	$\boldsymbol{U}_{41}$	$\boldsymbol{U}_{42}$	$\boldsymbol{U}_{52}$	$\boldsymbol{U}_{53}$	$\boldsymbol{U}_{63}$	$\boldsymbol{U}_{64}$	$\boldsymbol{U}_{14}$	$\boldsymbol{U}_{15}$	$\boldsymbol{U}_{25}$	$\boldsymbol{U}_{26}$	$\boldsymbol{U}_{36}$
$\Delta P_p > 0$	$\Delta Q_p < 0$	$\boldsymbol{U}_{15}$	$\boldsymbol{U}_{25}$	$\boldsymbol{U}_{26}$	$\boldsymbol{U}_{36}$	$\boldsymbol{U}_{31}$	$\boldsymbol{U}_{41}$	$\boldsymbol{U}_{42}$	$\boldsymbol{U}_{52}$	$\boldsymbol{U}_{53}$	$\boldsymbol{U}_{63}$	$\boldsymbol{U}_{64}$	$\boldsymbol{U}_{14}$
$\Delta P_p < 0$	$\Delta Q_p > 0$	$\boldsymbol{U}_{42}$	$\boldsymbol{U}_{52}$	$\boldsymbol{U}_{53}$	$\boldsymbol{U}_{63}$	$\boldsymbol{U}_{64}$	$\boldsymbol{U}_{14}$	$\boldsymbol{U}_{15}$	$\boldsymbol{U}_{25}$	$\boldsymbol{U}_{26}$	$\boldsymbol{U}_{36}$	$\boldsymbol{U}_{31}$	$\boldsymbol{U}_{41}$
$\Delta P_p < 0$	$\Delta Q_p < 0$	$\boldsymbol{U}_{13}$	$\boldsymbol{U}_{14}$	$\boldsymbol{U}_{24}$	$\boldsymbol{U}_{25}$	$\boldsymbol{U}_{35}$	$\boldsymbol{U}_{36}$	$\boldsymbol{U}_{46}$	$\boldsymbol{U}_{41}$	$\boldsymbol{U}_{51}$	$\boldsymbol{U}_{52}$	$\boldsymbol{U}_{62}$	$\boldsymbol{U}_{63}$

that is, both active power P_p and reactive power Q_p should be increased, voltage vector $\boldsymbol{U}_{31}$ can be selected to increase P_p and Q_p. Other cases can be analogized, and the voltage-vector selection table is generated, as in Table I [25].

C. SMVS Controller Design

In order to reduce the tracking errors in active power P_p and reactive power Q_p, the switching function of SMVS controller is defined as $\mathbf{S} = [\,S_P \;\; S_Q\,]^T$, where

$$\begin{cases} S_P = \Delta P_p = P^*_{\mathrm{pref}} - P_p \\ S_Q = \Delta Q_p = Q^*_{\mathrm{pref}} - Q_p \end{cases}. \tag{6}$$

The control system should move along the sliding surface $\mathbf{S} = 0$, so as to accurately track the power references P^*_{pref} and Q^*_{pref}

$$\begin{cases} \dfrac{dS_P}{dt} = \dfrac{d\Delta P_p}{dt} = -\dfrac{dP_p}{dt} = 0 \\ \dfrac{dS_Q}{dt} = \dfrac{d\Delta Q_p}{dt} = -\dfrac{dQ_p}{dt} = 0 \end{cases}. \tag{7}$$

The rates of change in active and reactive powers can be obtained from (4)

$$\begin{cases} \frac{dP_p}{dt} = \dfrac{3}{2}\left(u_{p\alpha}\dfrac{di_{p\alpha}}{dt} + u_{p\beta}\dfrac{di_{p\beta}}{dt} + i_{p\alpha}\dfrac{du_{p\alpha}}{dt} + i_{p\beta}\dfrac{du_{p\beta}}{dt}\right) \\ \frac{dQ_p}{dt} = \dfrac{3}{2}\left(-u_{p\alpha}\dfrac{di_{p\beta}}{dt} + u_{p\beta}\dfrac{di_{p\alpha}}{dt} + i_{p\alpha}\dfrac{du_{p\beta}}{dt} - i_{p\beta}\dfrac{du_{p\alpha}}{dt}\right) \end{cases} \tag{8}$$

where

$$\begin{cases} u_{p\alpha} = U_{pm}\cos(\omega_p t) \\ u_{p\beta} = U_{pm}\sin(\omega_p t) \end{cases} \tag{9}$$

where U_{pm} is the amplitude of the output voltage of the power winding. Then the derivatives of the grid voltage are

$$\begin{cases} \dfrac{du_{p\alpha}}{dt} = -\omega_p u_{p\beta} \\ \dfrac{du_{p\beta}}{dt} = \omega_p u_{p\alpha} \end{cases}. \tag{10}$$

TABLE II
PARAMETERS OF THE OW-BDFRG

Parameter	Value
Rated power (kW)	42
Rated voltage (V)	380
Rated current (A)	44.2
Pole-pairs number of power winding	3
Pole-pairs number of control winding	1
Resistance of power winding (Ω)	0.1662
Resistance of control winding (Ω)	0.1882
Self-inductance of power winding (mH)	17.37
Self-inductance of control winding (mH)	23.51
Mutual-inductance between the two stator windings (mH)	18.13
Moment of inertia (kg·m^2)	0.3

The rates of change in the power winding current can be derived from (1)

$$\begin{cases} \dfrac{di_{p\alpha}}{dt} = \dfrac{1}{\sigma L_p}\Big[u_{p\alpha} - R_p i_{p\alpha} + \left(\omega_p L_p + \omega_c \dfrac{L_m^2}{L_c}\right) i_{p\beta} \\ \qquad - \dfrac{L_m}{L_c}\left(u_{c\alpha} - R_c i_{c\alpha}\right) - \omega_r L_m i_{c\beta}\Big] \\ \dfrac{di_{p\beta}}{dt} = \dfrac{1}{\sigma L_p}\Big[u_{p\beta} - R_p i_{p\beta} - \left(\omega_p L_p + \omega_c \dfrac{L_m^2}{L_c}\right) i_{p\alpha} \\ \qquad + \dfrac{L_m}{L_c}\left(u_{c\beta} - R_c i_{c\beta}\right) - \omega_r L_m i_{c\alpha}\Big] \end{cases} \tag{11}$$

where $\sigma = 1 - L_m^2/L_p L_c$ is the leakage factor.

Equation (8) can be rewritten by substituting (10) and (11) into (8)

$$\begin{cases} \dfrac{dP_p}{dt} = \dfrac{3}{2}\dfrac{1}{\sigma L_p}\Big\{u_{p\alpha}^2 + u_{p\beta}^2 - \omega_r L_m\left(u_{p\alpha} i_{c\beta} + u_{p\beta} i_{c\alpha}\right) \\ \qquad - \dfrac{L_m}{L_c}\left[u_{p\alpha}\left(u_{c\alpha} - R_c i_{c\alpha}\right) - u_{p\beta}\left(u_{c\beta} - R_c i_{c\beta}\right)\right]\Big\} \\ \qquad - \dfrac{R_p}{\sigma L_p} P_p - \left[\omega_p\left(1 + \dfrac{1}{\sigma}\right) + \omega_c \dfrac{L_m^2}{\sigma L_p L_c}\right] Q_p \\ \dfrac{dQ_p}{dt} = \dfrac{3}{2}\dfrac{1}{\sigma L_p}\Big\{\omega_r L_m\left(u_{p\alpha} i_{c\alpha} - u_{p\beta} i_{c\beta}\right) \\ \qquad - \dfrac{L_m}{L_c}\left[u_{p\alpha}\left(u_{c\beta} - R_c i_{c\beta}\right) + u_{p\beta}\left(u_{c\alpha} - R_c i_{c\alpha}\right)\right]\Big\} \\ \qquad + \left[\omega_p\left(1 + \dfrac{1}{\sigma}\right) + \omega_c \dfrac{L_m^2}{\sigma L_p L_c}\right] P_p - \dfrac{R_p}{\sigma L_p} Q_p \end{cases}. \tag{12}$$

The rates of change in active and reactive powers is given by

$$\frac{d\mathbf{S}}{dt} = \begin{bmatrix} -\dfrac{dP_p}{dt} \\ -\dfrac{dQ_p}{dt} \end{bmatrix} = \mathbf{F} + \mathbf{D}\mathbf{U}_c \tag{13}$$

where

$$\mathbf{F} = \begin{bmatrix} F_P \\ F_Q \end{bmatrix} = \frac{3}{2}\frac{L_m}{\sigma L_p}\left\{\omega_r \begin{bmatrix} u_{p\beta} & u_{p\alpha} \\ -u_{p\alpha} & u_{p\beta} \end{bmatrix} - \frac{R_c}{L_c}\begin{bmatrix} u_{p\alpha} & -u_{p\beta} \\ u_{p\beta} & u_{p\alpha} \end{bmatrix}\right\}$$
$$\times \begin{bmatrix} i_{c\alpha} \\ i_{c\beta} \end{bmatrix}$$
$$+ \begin{bmatrix} \frac{R_p}{\sigma L_p} & \omega_p\left(1+\frac{1}{\sigma}\right) + \omega_c \frac{L_m^2}{\sigma L_p L_c} \\ -\left[\omega_p\left(1+\frac{1}{\sigma}\right) + \omega_c \frac{L_m^2}{\sigma L_p L_c}\right] & \frac{R_p}{\sigma L_p} \end{bmatrix}$$
$$\times \begin{bmatrix} P_p \\ Q_p \end{bmatrix} - \frac{3}{2}\frac{1}{\sigma L_p}\begin{bmatrix} u_{p\alpha}^2 + u_{p\beta}^2 \\ 0 \end{bmatrix} \tag{14}$$

$$\mathbf{D} = \frac{3}{2}\frac{L_m}{\sigma L_p L_c}\begin{bmatrix} u_{p\alpha} & -u_{p\beta} \\ u_{p\beta} & u_{p\alpha} \end{bmatrix} \tag{15}$$

$$\mathbf{U}_c = \begin{bmatrix} u_{c\alpha} & u_{c\beta} \end{bmatrix}^T \tag{16}$$

The common exponential reaching law is used to design the SMVS controller [26], then

$$\mathbf{U}_c = \begin{bmatrix} u_{c\alpha} \\ u_{c\beta} \end{bmatrix} = -\mathbf{D}^{-1}\begin{bmatrix} F_P + k_1 S_P + k_2 \mathrm{sat}\left(S_P\right) \\ F_Q + k_3 S_Q + k_4 \mathrm{sat}\left(S_Q\right) \end{bmatrix} \tag{17}$$

where $k_1 \sim k_4$ are all the positive control constants,$\mathrm{sat}(\cdot)$ is the saturation function and is given in (18). The saturation function is used instead of the sign function to reduce the high-frequency chattering caused by the rapid switching and some uncertain factors

$$\mathrm{sat}\left(S_i\right) = \begin{cases} 1, \ S_i > \lambda_i \\ S_i/\lambda_i, |S_i| \leq \lambda_i \\ -1, \ S_i < -\lambda_i \end{cases} \tag{18}$$

where λ_i is the error band (a positive control constant), and the subscript $i = P, Q$.

To prove the stability of control system, the Lyapunov function is used

$$\boldsymbol{V} = \frac{1}{2}\mathbf{S}^T\mathbf{S} = \frac{1}{2}\left(S_P^2 + S_Q^2\right) \tag{19}$$

$$\frac{d\mathbf{V}}{dt} = S_P\frac{dS_P}{dt} + S_Q\frac{dS_Q}{dt} = \mathbf{S}^T\frac{d\mathbf{S}}{dt}. \tag{20}$$

Substituting (13) into (20)

$$\frac{d\mathbf{V}}{dt} = \mathbf{S}^T\left(\mathbf{F} + \mathbf{D}\mathbf{U}_c\right). \tag{21}$$

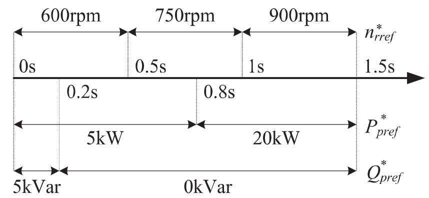

Fig. 5. Step changes in given parameters.

Substituting (17) into (21)

$$\frac{d\mathbf{V}}{dt} = \begin{bmatrix} S_P & S_Q \end{bmatrix}$$
$$\times \left(\begin{bmatrix} F_P \\ F_Q \end{bmatrix} + \mathbf{D}\left(-\mathbf{D}^{-1}\begin{bmatrix} F_P + k_1 S_P + k_2\mathrm{sat}\left(S_P\right) \\ F_Q + k_3 S_Q + k_4\mathrm{sat}\left(S_Q\right) \end{bmatrix}\right)\right)$$
$$= \begin{bmatrix} S_P & S_Q \end{bmatrix}\begin{bmatrix} -k_1 S_P - k_2\mathrm{sat}\left(S_P\right) \\ -k_3 S_Q - k_4\mathrm{sat}\left(S_Q\right) \end{bmatrix}$$
$$= -k_1 S_P^2 - k_2 S_P\mathrm{sat}\left(S_P\right) - k_3 S_Q^2 - k_4 S_Q\mathrm{sat}\left(S_Q\right) \tag{22}$$

when $S_P \neq 0$ and $S_Q \neq 0$, $k_1 S_P^2 > 0$, $k_2 S_Q^2 > 0$, $k_3 S_P sat(S_P) > 0$, and $k_4 S_Q sat(S_Q) > 0$ always hold true, so does $d\mathbf{V}/dt < 0$.

When $S_P \neq 0$ and $S_Q \neq 0$

$$\mathbf{V} = \frac{1}{2}\mathbf{S}^T\mathbf{S} = \frac{1}{2}\left(S_P^2 + S_Q^2\right) > 0. \tag{23}$$

Since $\boldsymbol{V}$ is positive definite, and $d\boldsymbol{V}/dt$ is negative definite, the control system is asymptotically stable according to the second rule of Lyapunov.

IV. Simulation Analysis

The proposed system is first modeled in MATLAB/Simulink software. The generator parameters are tabulated in Table II.

In order to analyze the power tracking effect and verify the superiority of the proposed system, the power regulation of a typical DPC-based BDFRG system and the proposed SMVS-DPC-based OW-BDFRG system is compared at subsynchronous, synchronous, and supersynchronous conditions. The step changes in relation to speed, active, and reactive power are presented in Fig. 5.

Figs. 6 and 7 present the simulation results of the typical DPC-based BDFRG system and the proposed SMVS-DPC-based OW-BDFRG system, including the currents waveforms of the power winding and control winding, and the waveforms of active and reactive powers. It can be seen from Fig. 6 that the power tracking effect of the typical DPC method under subsynchronous operation is worse and the distortion of the power winding output current waveform is larger. More spikes occur in the active power waveform and its error is as much as 5 kW. It is difficult to control the power in the given error range using a hysteresis method of typical DPC control. The performance of the typical DPC method under synchronous and supersynchronous operation is acceptable, but the one under subsynchronous operation is unsatisfactory. The simulation results in Fig. 7 show that for the SMVS-DPC-based OW-BDFRG

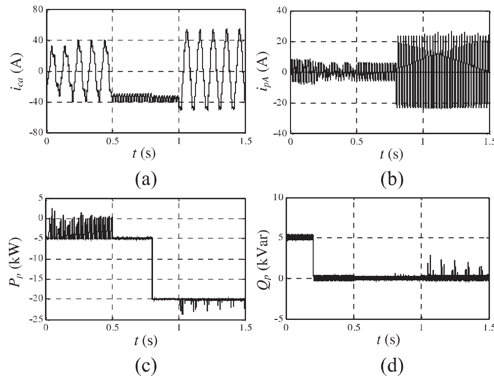

Fig. 6. Simulation results of a typical DPC-based BDFRG system. (a) Phase-a current in the control winding. (b) Phase-a current in the power winding. (c) Active power. (d) Reactive power.

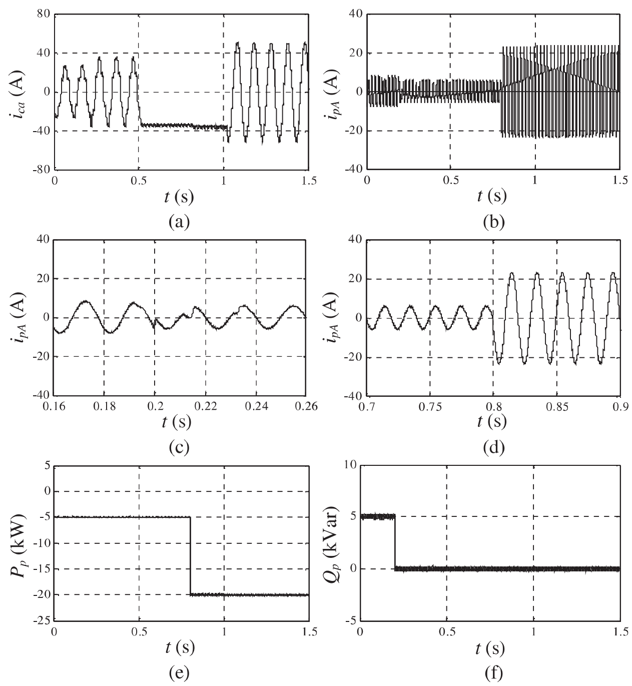

Fig. 7. Simulation results of the SMVS-DPC-based OW-BDFRG system. (a) Phase-a current in the control winding. (b) Phase-a current in the power winding. (c) Enlarged waveform of phase-a current in the power winding. (d) Enlarged waveform of phase-a current in the power winding. (e) Active power. (f) Reactive power.

system, the power tracking effect under subsynchronous, synchronous, and supersynchronous operations are all excellent. Its active power and reactive power can track the given values accurately and the errors are both small (±200 W/Var). From the enlarged phase-A current in the power winding in Fig. 7(c) and (d), the output current frequency of the power winding can be kept at 50 Hz and the variable-speed constant-frequency operation can be achieved. The fluctuation of power winding output current is less than the previous case. Obviously, the proposed SMVS-DPC-based OW-BDFRG system is superior to the typical DPC-based BDFRG system in the aspect of power tracking performance.

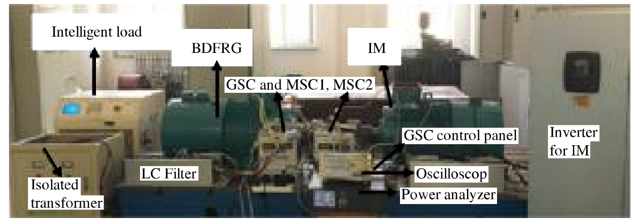

Fig. 8. Experimental platform of the SMVS-DPC-based OW-BDFRG system.

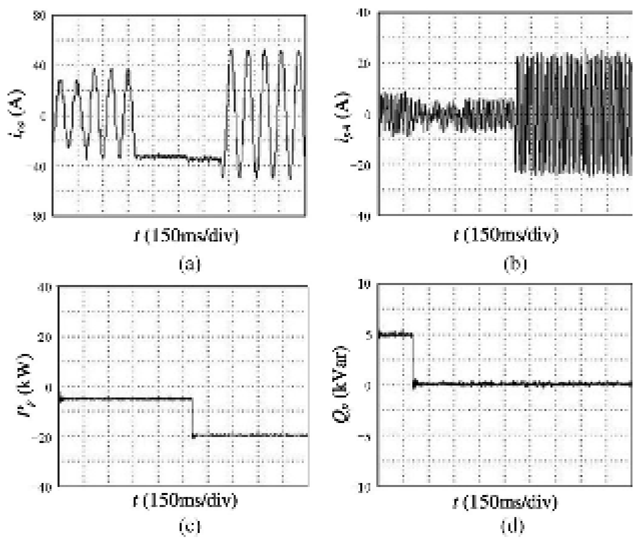

Fig. 9. Dynamic experimental results of the SMVS-DPC-based OW-BDFRG system. (a) Phase-a current in the control winding. (b) Phase-a current in the power winding. (c) Active power. (d) Reactive power.

V. Experimental Results

An experimental platform of the SMVS-DPC-based OW-BDFRG system is set up, shown in Fig. 8. An induction motor and its inverter are taken as the prime motor to simulate the actual wind turbine. The rated capacity of one converter is 15 kW. The power switching devices adopt Infineon high-speed insulated gate bipolar transistor (IGBT) power module (FF75R12RT4). The main controller core is DSP TMS320F28335. The accuracy of the current sector (LT58-S7) is ±0.8%.

The reference values of speed, active, and reactive powers are the same as in Fig. 5. Experimental results are obtained, as shown in Figs. 9–12. Fig. 9 shows the dynamic experimental results of the SMVS-DPC-based OW-BDFRG system. Fig. 10 presents the currents in the power winding and control winding as well as the active and reactive powers under the subsynchronous operation when $n^*_{r\mathrm{ref}} = 600$ r/min, $P^*_{p\mathrm{ref}} = 5$ kW, and $Q^*_{p\mathrm{ref}} = 5$ kVar. Fig. 11 presents the same waveforms under the synchronous operation when $n^*_{r\mathrm{ref}} = 750$ r/min, $P^*_{p\mathrm{ref}} = 5$ kW, and $Q^*_{p\mathrm{ref}} = 0$ kVar. Fig. 12 shows results under the super-synchronous operation when $n^*_{r\mathrm{ref}} = 900$ r/min, $P^*_{p\mathrm{ref}} = 20$ kW, and $Q^*_{p\mathrm{ref}} = 0$ kVar.

It can be seen from Figs. 9–12 that the experimental results agree well with the theoretical analysis and simulation results.

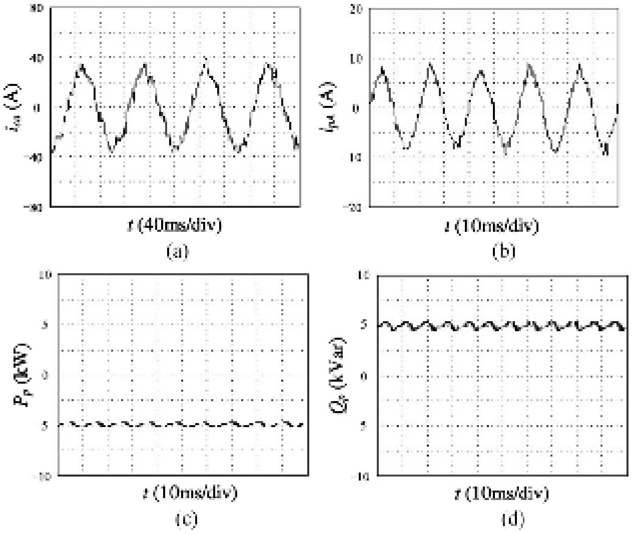

Fig. 10. Experimental results of the SMVS-DPC-based OW-BDFRG system when, $n^*_{rref} = 600$ rpm, $P^*_{pref} = 5$ kW, and $Q^*_{pref} = 5$ kVar. (a) Phase-a current in the control winding. (b) Phase-a current in the power winding. (c) Active power. (d) Reactive power.

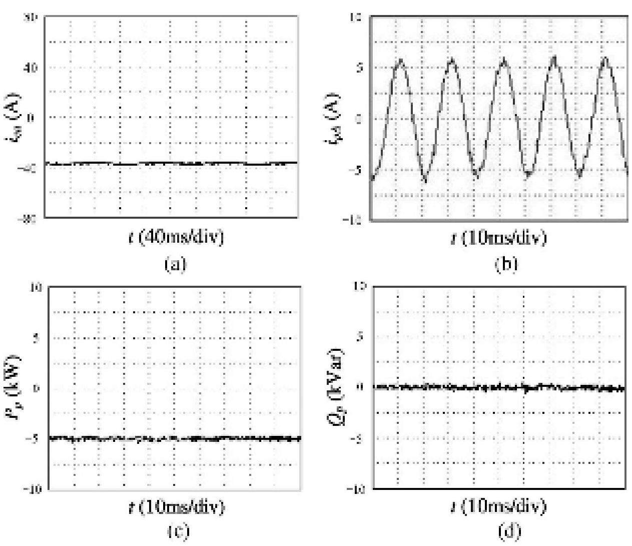

Fig. 11. Experimental results of the SMVS-DPC-based OW-BDFRG system when $n^*_{\text{rref}} = 750$ r/min, $P^*_{\text{pref}} = 5$ kW, and $Q^*_{\text{pref}} = 0$ kVar. (a) Phase-a current in the control winding. (b) Phase-a current in the power winding. (c) Active power. (d) Reactive power.

From Fig. 9, the transitions of the active and reactive powers change stably and rapidly from some values to another, and the active and reactive powers can follow the given values accurately with low fluctuations under subsynchronous, synchronous, and supersynchronous operations, which verifies that the proposed SMVS-DPC-based OW-BDFRG system has good dynamic performance. From Figs. 10–12, the fluctuations of active and reactive powers are within the control range, and the output current frequency of the OW-BDFRG power winding can be kept at 50 Hz by adjusting the excitation current frequency of the control winding. The experimental results show that the

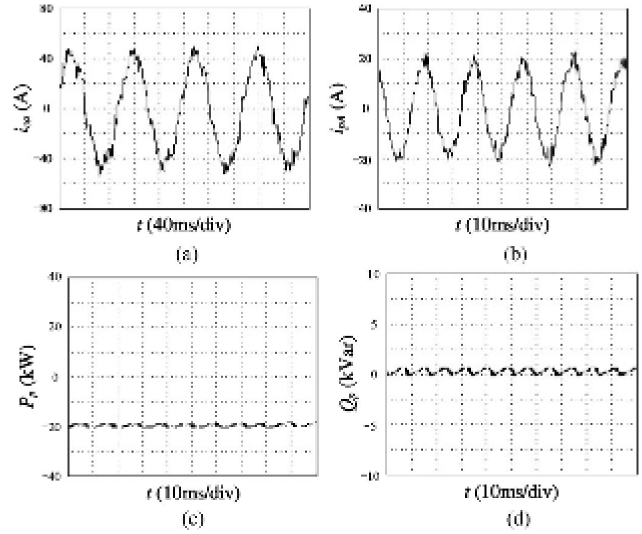

Fig. 12. Experimental results of the SMVS-DPC-based OW-BDFRG system when $n^*_{\text{rref}} = 900$ r/min, $P^*_{\text{pref}} = 20$ kW, and $Q^*_{\text{pref}} = 0$ kVar. (a) Phase-a current in the control winding. (b) Phase-a current in the power winding. (c) Active power. (d) Reactive power waveform.

proposed SMVS-enhanced DPC scheme can enable the output active and reactive powers of the OW-BDFRG system to rapidly and accurately track the given power values and implement the variable-speed constant-frequency operation.

VI. Conclusion

This paper has presented a novel OW-BDFRG with dual two-level converters controlled by an SMVS-enhanced DPC method, which requires lower converter rating and switching frequency, and has simpler control structure, more flexible control mode, and better operation performance and fault redundancy capability. The proposed SMVS-DPC-based OW-BDFRG system not only has the good control effect of the power tracking, but also can implement the variable-speed constant-frequency operation. The superiority of the proposed system has been verified through simulation and experimental results. The output current frequency, active, and active and reactive powers of the proposed OW-BDFRG are all excellent under subsynchronous, synchronous, and super-synchronous conditions. The developed technologies are particularly suited for high-power wind turbine applications where the variable-speed constant-frequency is required as well as good dynamic performance.

References

[1] H. Gorginpour, H. Oraee, and E. Abdi, “Calculation of core and stray load losses in brushless doubly fed induction generators,” *IEEE Trans. Ind. Electron.*, vol. 61, no. 7, pp. 3167–3177, Jul. 2014.

[2] E. Abdi *et al.*, “Performance analysis and testing of a 250 kW medium-speed brushless doubly-fed induction generator,” *IET Renew. Power Gener.*, vol, 7, no. 6, pp. 631–638, Nov. 2013.

[3] M. Cheng and Y. Zhu, “The state of the art of wind energy conversion systems and technologies: A review,” *Energy Convers. Manage.*, vol. 88, pp. 332–347, 2014.

[4] R. Mcmahon, P. Tavner, E. Abdi, P. Malliband, and D. Barker, “Characterising brushless doubly fed machine rotors,” *IET Elect. Power Appl.*, vol. 7, no. 7, pp. 535–543, Aug. 2013.

[5] Y. Wang, T. A. Lipo, and D. Pan, "Half-controlled-converter-fed open-winding permanent magnet synchronous generator for wind applications," in *Proc. 14th Int. Power Electron. Motion Control Conf.*, Ohrid, Macedonia, Sep. 2010, pp. T4-123–T4126.

[6] Y. J. Zhou and H. Nian, "Zero-sequence current suppression strategy of open-winding PMSG system with common DC bus based on zero vector redistribution," *IEEE Trans. Ind. Electron.*, vol. 62, no. 6, pp. 3399–3408, Jun. 2015.

[7] H. Nian and Y. J. Zhou, "Investigation of open-winding PMSG system with the integration of fully controlled and uncontrolled converter," *IEEE Trans. Ind. Appl.*, vol. 51, no. 1, pp. 429–439, Jan./Feb. 2015.

[8] D. Pan, Y. Wang, and T. A. Lipo, "A series regulated open-winding PM generator based constant voltage, variable frequency AC distribution system," in *Proc. IEEE ECCE Asia Downunder*, Melbourne, Vic., Australia, Jun. 2013, pp. 214–220.

[9] Q. T. Deng, J. D. Wei, B. Zhou, C. Han, and C. C. Chen, "Research on control strategies of open-winding permanent magnetic generator," in *Proc. 2011 Int. Conf. Elect. Mach. Syst.*, Beijing, China, Aug. 2011, pp. 1–6.

[10] S. Ademi and M. G. Jovanovi, "Vector control methods for brushless doubly fed reluctance machines," *IEEE Trans. Ind. Electron.*, vol. 62, no. 1, pp. 96–104, Jan. 2015.

[11] Z. S. Jiang, S. Wang, and X. P. Ru, "Simulation study of vector control strategy for stand-alone BDFG system," *Micromotors*, vol. 47, no. 2, pp. 48–51, 2014.

[12] K. Ji, S. H. Huang, J. Zhu, Y. Gao, and C. Zeng, "Vector control and synchronization of brushless doubly-fed machine for high power wind power generation," in *Proc. 15th Int. Conf. Elect. Mach. Syst.*, Sapporo, Japan, Oct. 2012, pp. 1–6.

[13] S. Ademi, M. G. Jovanovic, and M. Hasan, "Control of brushless doubly-fed reluctance generators for wind energy conversion systems," *IEEE Trans. Energy Convers.*, vol. 30, no. 2, pp. 596–604, Jun. 2015.

[14] S. Y. Shao, E. Abdi, F. Barati, and R. McMahon, "Stator-flux-oriented vector control for brushless doubly fed induction generator," *IEEE Trans. Ind. Electron.*, vol. 56, no. 10, pp. 4220–4228, Oct. 2009.

[15] Y. G. Zhu, X. Zhang, Z. Xie, and S. Y. Yang, "Simulation study on speed sensorless vector control of brushless doubly-fed wind power generator," *Acta Energiae Solaris Sinica*, vol. 34, no. 3, pp. 496–502, 2013.

[16] B. Li and S. Liu, "Study on direct torque control strategy of brushless doubly-fed induction generator for wind power generation," *J. Comput. Inf. Syst.*, vol. 10, no. 24, pp. 10389–10396, 2014.

[17] X. J. Yao, B. H. Zhang, S. R. Wang, Q. D. Guo, and H. Chen, "Anti-ripple fuzzy DTC strategy of brushless doubly-fed wind power generation system based DSVM," *Renew. Energy Resour.*, vol. 31, no. 4, pp. 55–59, 2013.

[18] S. Jin, F. G. Zhang, and L. C. Zhu, "VSCF maximal power tracking for brushless doubly fed wind power generator," *Acta Energiae Solaris Sinica*, vol. 35, no. 11, pp. 2279–2286, 2014.

[19] W. K. Song and D. G. Dorrell, "Implementation of improved direct torque control method of brushless doubly-fed reluctance machines for wind turbine," in *Proc. IEEE Int. Conf. Ind. Technol.*, Busan, South Korea, Mar. 2014, pp. 509–513.

[20] H. R. Mosaddegh and H. A. Zarchi, "Variable structure direct torque control of brushless doubly fed induction generator for wind turbine applications," in *Proc. 22nd Iranian Conf. Elect. Eng.*, Tehran, Iran, May 2014, pp. 671–676.

[21] S. M. Li, H. H. He, Y. K. Zhang, and Y. Zheng, "A sliding mode variable structure-based direct power control strategy for doubly fed induction generator," *Power Syst. Technol.*, vol. 37, no. 7, pp. 2006–2010, 2013.

[22] H. Chaal and M. Jovanovic, "Direct power control of brushless doubly-fed reluctance machines," in *Proc. 5th IET Int. Power Electron., Mach. Drives*, Brighton, U.K., Apr. 2010, pp. 1–6.

[23] S. Di Gennaro, J. Rivera Dominguez, and M. A. Meza, "Sensorless high order sliding mode control of induction motors with core loss," *IEEE Trans. Ind. Electron.*, vol. 61, no. 6, pp. 2678–2689, Jun. 2014.

[24] T. Bernardes, V. F. Montagner, H. A. Grundling, and H. Pinheiro, "Discrete-time sliding mode observer for sensorless vector control of permanent magnet synchronous machine," *IEEE Trans. Ind. Electron.*, vol. 61, no. 4, pp. 1679–1691, Apr. 2014.

[25] S. Jin, L. Shi, L. Zhu, T. Dong, F. Zhang, and W. Cao, "Performance comparison of direct power control for brushless doubly-fed wind power generator with different control winding structure," in *Proc. IEEE Transport. Electrific. Conf. Expo. Asia-Pacific*, Busan, South Korea, Jun. 1–4, 2016, pp. 261–266.

[26] J. K. Liu, *MATLAB Simulation of Sliding Mode Variable Structure Control*. Beijing, China: Tsinghua Univ. Press, 2005.

Shi Jin (M'2017) was born in 1981. She received the B.E., M.S., and Ph.D. degrees from the Shenyang University of Technology, Shenyang, China, in 2004, 2007, and 2011, respectively, all in electrical engineering.

Since 2011, she has been a Teacher with the School of Electrical Engineering, Shenyang University of Technology. Her research and teaching interests include power electronic technology, electrical machines and their control systems, and wind power generation. She has authored or co-authored 41 papers published in important academic journals and presented at domestic and international conferences, of which 32 were cited by SCI/EI.

Dr. Jin has received financial aid from the National Natural Science Foundation of China for her research project "Open-Winding Brushless Doubly-Fed Wind Power Generator With Hybrid Rotor and its Direct Power Control Strategy" (Grant 51277124). She was selected as for the Baiqianwan Talents Project of Liaoning Province in 2013.

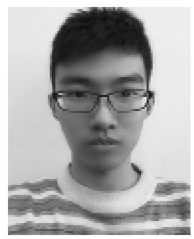

Long Shi was born in 1992. He received the B.S. degree in electrical engineering from the Shenyang University of Technology, Shenyang, China, in 2015. He is currently working toward the M.S. degree in fault-tolerant control strategy of open-winding brushless doubly-fed wind power generator based on dual three-level converters from the School of Electrical Engineering, Shenyang University of Technology.

His research interests include power electronics and power transmission, special motors and their control, and wind power generators and their control.

Liancheng Zhu was born in 1979. He received the B.S. and M.S. degrees in industry electric automation and control theory and control engineering from the University of Science and Technology, Liaoning, Anshan, China, in 2002 and 2007, respectively. He is currently working toward the Ph.D. degree in direct power control strategy for open-winding brushless doubly-fed wind power generator with hybrid rotor from the School of Electrical Engineering, Institute of Electric Control Technology, Shenyang University of Technology, Shenyang, China.

Since 2002, he has also been a Teacher with the School of Electronic and Information Engineering, University of Science and Technology. His research interests include power electronics and power transmission, special motors and their control, and wind power generators and their control.

Wenping Cao (SM'11) received the B.Eng. degree in electrical engineering from Beijing Jiaotong University, Beijing, China, in 1991, and the Ph.D. degree in electrical machines and drives from the University of Nottingham, Nottingham, U.K., in 2004.

He is currently a Chair Professor of Electrical Power Engineering and the Head of Power Electronics, Machines and Power System Group with Aston University, Birmingham, U.K.

Dr. Cao is currently a Royal Society Wolfson Research Merit Award holder, U.K. He was a semifinalist at the Annual MIT-CHIEF Business Plan Contest, USA, in 2015; the Dragon's Den Competition Award winner from Queen's University Belfast, U.K., in 2014; and the Innovator of the Year Award winner from Newcastle University, U.K., in 2013. He received the Best Paper Award at the 2013 International Symposium on Linear Drives for Industry Applications. He serves as an Editor for the IEEE TRANSACTIONS ON POWER ELECTRONICS, the IEEE TRANSACTIONS ON INDUSTRY APPLICATIONS, IEEE INDUSTRY APPLICATIONS MAGAZINE, *IET Power Electronics*, and *Electric Power Components and Systems*. He is also the Chief Editor for five Special Issues and four books. He is currently the Chairman for the Industrial Electronics Society, and the IEEE U.K. and Ireland Sections.

Ting Dong was born in 1982. She received the B.E. and Ph.D. degrees from the Shenyang University of Technology, Shenyang, China, in 2004 and 2010, respectively, all in electrical engineering.

Since 2011, she has been a Teacher with the School of Electrical Engineering, Shenyang University of Technology. Her research interests include is direct-drive motor used in advanced equipment manufacturing and electric vehicle, such as phase modulation torque motor, inductor motor, brushless dc motor (BLDC), and so on. She has authored or co-authored 13 patents, and more than 10 papers published in important academic journals and presented at domestic and international conferences.

Dr. Dong has received the National Natural Science Foundation of China Research on Magnetic Field Characteristics and Torque Performance of Permanent Magnetic Torque Motor with Similar Pole Number and Slot Number Made by Oriented Silicon Steel Sheet Grant 51607116. She was selected as the Baiqianwan Talents Project of Liaoning Province in 2015.

Fengge Zhang (M'17) was born in 1963. He received the B.E.E., M.S., and Ph.D. degrees from the Shenyang University of Technology, Shenyang, China, in 1984, 1990, and 2000, respectively, all in electrical engineering.

Since 1984, he has been a Teacher with the School of Electrical Engineering, Shenyang University of Technology, where he is currently a Professor. From October 2001 to July 2002, he was a Visiting Scholar at Esslingen University of Applied Sciences, Esslingen, Germany. For the last several years, he has published numerous papers in important international conference proceedings and journals on electrical machines and control systems. His research and teaching interests include electric–magnetic theory, dynamic simulation, magnetic field analysis, optimized design, computer control technology of electrical machines, and wind power generating systems. He is also active in the area of power converters for variable speed control and drive systems.

Dr. Zhang received six paper awards from Liaoning Province and four research awards from the National Machine Industry Ministry, Liaoning Province and Shenyang City, for his outstanding research accomplishments from various research projects completed in recent years. He has been confirmed as a Young Academic Skeleton by Liaoning Province and National Machine Industry Ministry. He received financial aid from the National Natural Science Foundation of China for his research project "Magnetic Field Modulation Doubly-Fed Brushless AC Machine," and from Liaoning Province and others.